Discover Oncology

RESEARCH Open Access

A differential single-cell transcriptome atlas of left-sided and right-sided colorectal cancer

Chengzhi Zhao[1,2†], Weiye Zhou[1†], Guangjian Zeng[1], Yeen Huang[1], Chuan Shi[1], Haibei Ma[1], Yang Li[3], Jiachun Lv[4], Xiaohua Liang[5*] and Shenying Fang[1*]

[†]Chengzhi Zhao and Weiye Zhou contributed equally to this work.

*Correspondence:
Xiaohua Liang
xiaohualiang@hospital.cqmu.edu.cn
Shenying Fang
Fangsy@sustech.edu.cn

Full list of author information is available at the end of the article

Abstract

Left-sided colorectal cancer (LCRC) and right-sided colorectal cancer (RCRC) show marked differences in prognosis and therapeutic response, yet the underlying molecular mechanisms remain poorly understood. We hypothesize that these clinical differences reflect distinct cell-type-specific transcriptional programs and microenvironmental interactions that can be resolved at single-cell resolution. To test this hypothesis, this study analyzed single-cell transcriptomic data from 16 colorectal cancer (CRC) patients (8 LCRC and 8 RCRC), revealing molecular differences between LCRC and RCRC in tumor cells, T cells, B cells, myeloid cells, fibroblasts, and endothelial cells, and constructing a differential atlas of LCRC versus RCRC. Significant molecular and cellular differences were observed between LCRC and RCRC. *MTRNR2L8* was markedly upregulated in RCRC tumor cells and associated with poorer patient survival, potentially regulated by transcription factors *STAT3*, *ELK3*, and *EP300*. RCRC showed an increased proportion of the CD8-EFFECTOR 3 subpopulation, which co-expresses effector and exhaustion markers, suggesting favorable immunotherapy response. In contrast, the CD4-heat shock proteins (CD4-HSP) subpopulation was almost exclusively present in LCRC, suggesting a potential correlation with a weaker response to immune checkpoint inhibitors. Additionally, *APP-CD74* ligand-receptor interactions were significantly enhanced in RCRC, potentially contributing to worse prognosis by inhibiting APP protein cleavage and promoting its accumulation. Validation was performed using an independent single-cell transcriptomic dataset, bulk RNA-seq data from TCGA CRC samples, and qPCR on locally collected CRC tissue specimens. In addition, a spatial transcriptomic dataset of CRC and immunohistochemistry data from the Human Protein Atlas (HPA) database were also used to validate part of the findings. This study provides a comprehensive single-cell transcriptomic atlas highlighting the molecular and cellular disparities between LCRC and RCRC, offering novel insights into tumor biology and informing the development of personalized therapeutic strategies.

Keywords Single-cell sequencing, Right-sided colorectal cancer, Left-sided colorectal cancer, Prognosis, Treatment response

1 Introduction

Colorectal cancer (CRC) is a multifactorial malignancy influenced by lifestyle, dietary habits, and genetic predisposition. It remains one of the most prevalent and lethal cancers worldwide [1]. CRC can be classified into left-sided colorectal cancer (LCRC) and right-sided colorectal cancer (RCRC) based on the site of tumor occurrence. Epidemiological studies have demonstrated that the prognosis of patients with RCRC is typically worse than that of patients with LCRC [2–4]. Moreover, the survival time and survival rate of patients with RCRC are significantly lower than those of patients with LCRC [5, 6]. Additionally, the genomic characteristics of LCRC and RCRC are completely different, with a high frequency of microsatellite instability (MSI) observed in RCRC patients, while chromosomal instability (CIN) is more prevalent in LCRC patients [7–10]. Furthermore, the treatment responses of RCRC and LCRC are entirely different. For LCRC, adjuvant chemotherapy and targeted therapies show better efficacy. However, for RCRC, immunotherapy demonstrates better effectiveness [11]. Nevertheless, the molecular mechanisms underlying the differences in prognosis and treatment responses between LCRC and RCRC have not been widely elucidated. This limitation hinders the exploration of targeted therapeutic approaches to improve the prognosis of LCRC and RCRC.

Single-cell RNA sequencing (scRNA-seq) can provide gene expression information at the single-cell resolution and has been extensively applied in cancer research in recent years. However, scRNA-seq studies directly interrogating the cellular programs underlying side-associated differences in CRC prognosis and therapy response remain limited. Here, we analyzed scRNA-seq data from 16 primary CRC tumors (8 LCRC and 8 RCRC) and identified side-associated molecular features across six major cell populations. We refer to this framework as a "differential atlas", defined as a single-cell reference map explicitly organized to highlight between-group differences (LCRC vs RCRC) in cell states, gene programs, pathway activities, and intercellular communication, rather than a generic cell census. To improve robustness, we validated key observations in an independent GEO scRNA-seq dataset (12 LCRC and 11 RCRC), together with TCGA bulk RNA-seq. In addition, we performed quantitative real-time PCR (qPCR) using locally collected CRC tissues to confirm expression patterns of selected genes. Together, this differential atlas provides a systematic resource for understanding side-associated biology in CRC and generates testable hypotheses for future mechanistic and translational studies.

2 Methods

2.1 Acquisition of scRNA-seq data

The single-cell sequencing data for the discovery cohort were obtained from the GEO database with registration number GSE200997 [12]. The dataset included a total of 23 samples, including 16 tumor samples and 7 normal para-cancer samples, from a total of 16 colorectal cancer patients. In addition, among the 16 tumor samples, 8 were from LCRC patients and 8 were from RCRC patients.

The single-cell sequencing data for the validation cohort for this study were obtained from the GEO database with registration number GSE132465 [13]. The dataset included a total of 23 samples, comprising 12 LCRC samples and 11 RCRC samples.

Detailed clinical and sample information for all patients included in both cohorts is summarized in Supplementary Table 2.

2.2 scRNA-seq data processing

The raw data we downloaded had undergone initial quality control, in which genes detected in fewer than three cells and cells expressing fewer than 200 genes were filtered out, and cells with > 25% mitochondrial gene content were removed. The original dataset comprised 16 tumor and 7 paracancerous samples. As our analysis was confined to interrogating differences between RCRC and LCRC, we excluded the 7 paracancerous samples and retained only the 16 tumor samples for subsequent analysis. The expression matrix, after removing the para-cancer samples, contained 23,828 genes and 31,586 cells, with an average of 1,974 cells per sample. "Seurat" (version 4.3.0) [14] software package was used for analysis of single-cell sequencing data. The depth of sequencing for each cell was first normalized using the "NormalizeData" function using the method "LogNormalize" and the parameter "scale.factor" using the default value 10000. Highly variable genes were identified using the "FindVariableFeatures" function with the "vst" method, selecting the top 2000 genes. The expression of all genes was normalized using the "ScaleData" function so that the distribution of the expression of each gene among different cells has a mean of 0 and a variance of 1. Additionally, the Python package "scanpy" [15] was used to visualize some of the dimensionality reduction results.

2.3 Clustering analysis

Principal Component Analysis (PCA) was applied to perform linear dimensionality reduction based on the 2000 highly variable genes obtained, and then the "FindNeighbors" function was used to construct a KNN graph based on Euclidean distances in the PCA space and optimize the distance weights based on the shared overlap of any two cells in their local neighborhoods. Clustering was performed using the "FindClusters" function, and the clustering results were visualized using the non-linear dimensionality reduction method t-distributed stochastic neighbor embedding (t-SNE) or uniform manifold approximation and projection (UMAP). Finally, these cell clusters were annotated to known cell types based on the marker genes expressed by each cell cluster. The reclustering of cell subpopulations was performed using a similar procedure but with slightly different PCA dimensions and "resolution" parameters.

2.4 Inference of tumor cells

The "infercnv" (version 1.6.0) R package (https://github.com/broadinstitute/inferCNV) was used to calculate CNV scores for epithelial cells. T and B cells, which exhibit normal levels of copy number variation, were used as reference populations. Epithelial cells were clustered together with T and B cells using k-means based on their CNV scores. Cells clustering with T/B cells were classified as normal epithelial cells, while the remaining epithelial cells were considered malignant (tumor cells). CNV scores of each cluster were visualized using violin plots with the "geom_violin" function in the R package "ggplot2".

2.5 Differential expression analysis and enrichment analysis

Differential expression analysis was performed using the "FindMarkers" and "FindAllMarkers" functions in Seurat. The parameters of differential genes were set to 0.25 for min.pct and 0.25 for logfc.threshold. Only genes with min.pct > 0.25 and logfc.threshold > 0.25 were identified as differential genes. The R package "clusterProfiler" (version

4.8.1) [16] was used to conduct Gene Ontology analysis and KEGG pathway enrichment analysis of differential genes to see what functions these differential genes mainly play.

2.6 Gene set variation analysis

The R package "GSVA" (version 1.46.0) [17] was used for gene set variation analysis of cell subpopulations to see differences in gene set expression between different cell subpopulations. The hallmark dataset used was downloaded from the https://www.gsea-msigdb.org/gsea/msigdb website. The resulting heatmap was generated by the R package "pheatmap" (version 1.0.12).

2.7 Pseudotime analysis

When performing pseudotime analysis on distinct subpopulations of tumor cells, the R packages "monocle" (version 2.26.0) [18], "monocle3" (version 1.3.4) [19], "CytoTRACE" (version 0.3.3) [20], and the Python package "phate" (version 1.0.11) [21] were utilized to identify differentiation relationships among various tumor cell subgroups. Moreover, the "BEAM" function within the monocle package was utilized to pinpoint pivotal genes at differentiation nodes. Subsequently, genes with a q-value below 1e-4 were chosen for Gene Ontology (GO) enrichment analysis, aiming to uncover the biological mechanisms governing differentiation among subpopulations of tumor cells.

2.8 Survival analysis

Survival analysis of differentially expressed genes identified between RCRC and LCRC patients was initially performed using GEPIA2 (http://gepia2.cancer-pku.cn/) [22] to explore their associations with patient prognosis. Specifically, the overall survival (OS) was conducted for the selected DEGs. In GEPIA2, the "Survival Analysis" module was employed. The patient cohort was automatically stratified into "High" and "Low" expression groups based on the median expression level of each queried gene within the TCGA-READ and TCGA-COAD datasets. The survival curves were generated using the Kaplan–Meier method, and the statistical significance of the difference between the two groups was assessed by the Log-rank test. A hazard ratio (HR) with 95% confidence interval (CI) and a Log-rank $P < 0.05$ were considered statistically significant.

To further evaluate whether *MTRNR2L8* was independently associated with patient outcomes, a multivariate Cox proportional hazards regression analysis was additionally performed in the TCGA-COAD cohort using the original clinical data and normalized transcriptomic expression values (TPM). This model adjusted for established clinicopathological variables, including age, gender, clinical stage, and treatment status. Adjusted hazard ratios (HRs) and 95% confidence intervals (CIs) were estimated, and $P < 0.05$ were considered statistically significant.

2.9 Single-cell regulatory network inference analysis

Using "pySCENIC" (version 0.12.1) [23], single-cell regulatory network inference analysis was performed on tumor cells from RCRC and LCRC, aiming to identify specific regulons that regulate RCRC and LCRC tumor cells, respectively. Co-expression analysis was performed using "GRNBoost2" to identify target genes co-expressed with the transcription factors and to obtain the co-expression network of the transcription factors and target genes. The identified co-expression networks were subsequently subjected to

motif analysis to distinguish between direct and indirect target genes. The reference co-expression module used (hg38__refseq-r80__10kb__up_and_down_tss.mc9nr.genes_vs_motifs.rankings.feather) was downloaded from https://resources.aertslab.org/cistarget/ website.

After obtaining the transcription factors specific to RCRC and LCRC tumor cells, a regulatory network of these transcription factors was constructed using "Cytoscape" software (version 3.9.1) [24].

2.10 Cell–cell communication analysis

Using the R package "CellChat" (version 1.6.0) [25], specific enrichment of ligand-receptor pairs was computed based on the expression levels of ligands and receptors within each cell cluster, followed by the analysis of communication between different cell clusters. Additionally, built-in functions within CellChat were used to visualize the communication patterns between various cell clusters.

2.11 Validation analysis using TCGA data

This study utilized bulk RNA-seq data from TCGA-READ and TCGA-COAD cohorts to assist in validating the differential analysis results. Based on the anatomical location of the samples, all cases were classified into LCRC (n = 297) and RCRC (n = 218). Differential gene expression analysis between LCRC and RCRC was performed using edgeR (version 3.40.2) [26], with differentially expressed genes identified based on a P-value threshold of < 0.05 and an absolute logFC greater than 0.4.

2.12 qPCR validation using tumor samples from a local CRC cohort

To validate the expression of *MTRNR2L8*, we performed quantitative real-time PCR (qPCR) on tumor tissue samples collected from a local cohort of 136 colorectal cancer patients. All specimens were obtained from the Second Affiliated Hospital of Guangzhou Medical University (Guangzhou, China). All patients were histologically diagnosed with CRC and had available tumor tissue samples preserved for molecular analysis. Key demographic and clinicopathological characteristics of this cohort are summarized in Supplementary Table 2. The internal reference gene and all primer sequences used for qPCR are provided in Supplementary Table 3.

Patients were stratified based on clinicopathological staging information. According to the American Joint Committee on Cancer (AJCC) staging system, there were 18 patients in stage I, 47 in stage II, 60 in stage III, and 11 in stage IV. Based on the T classification, 24 patients were categorized as T1–T2 and 112 patients as T3–T4. For nodal status, 68 patients were classified as N0, while the remaining 68 were classified as N1 or N2. Regarding distant metastasis, 125 patients were identified as M0 and 11 as M1.

2.13 Validation using spatial transcriptomic data

A spatial transcriptomic dataset of CRC (http://www.cancerdiversity.asia/scCRLM/) [27] was analyzed to validate the presence of the CD8-EFFECTOR 3 subpopulation. Co-expression patterns of immune activation genes (such as *CXCL13* and *PRF1*) and immune exhaustion genes (such as *PDCD1* and *CD96*) were examined within the tumor microenvironment.

2.14 Validation using immunohistochemistry data from HPA database

To further validate gene expression patterns at the protein level, immunohistochemistry (IHC) data were retrieved from the HPA database [28]. Protein expression levels of selected key genes were examined in colorectal tumor tissues and matched normal tissues.

3 Results

3.1 Overview of the differential atlas of LCRC and RCRC

The discovery cohort comprised single-cell transcriptomic profiles from 16 tumor samples (8 LCRC and 8 RCRC). After excluding 7 paracancerous samples, a total of 31,586 cells were retained for downstream analysis. Dimensionality reduction and clustering identified six major cell types—epithelial cells, T cells, B cells, myeloid cells, fibroblasts, and endothelial cells—each exhibiting distinct transcriptional profiles (Fig. 1).

Based on a number of well-recognized marker genes, we annotated these six cell clusters as known cell types, including epithelial cells, T cells, B cells, myeloid cells, fibroblasts, and endothelial cells. All marker genes were expressed only in specific cell groups (Supplementary Fig. 1). These six cell types were present in both LCRC and RCRC samples, with endothelial cells, fibroblasts, myeloid cells, and B cells comprising similar proportions in both LCRC and RCRC, whereas the proportions of epithelial cells and T cells differed markedly between the two groups. Furthermore, the cellular composition varied substantially across individual patients. (Supplementary Fig. 2).

3.2 Overall differences in tumor cells between LCRC and RCRC

We identified epithelial cells from the entire cell population using specific marker genes of epithelial cells, such as *EPCAM* and *KRT18*. These two genes show high-specific expression in epithelial cells, with minimal expression observed in other cell populations (Fig. 2A).

Based on the annotated epithelial cells, we employed inferCNV to infer copy number variation (CNV) status and identify malignant epithelial cells within the epithelial cell

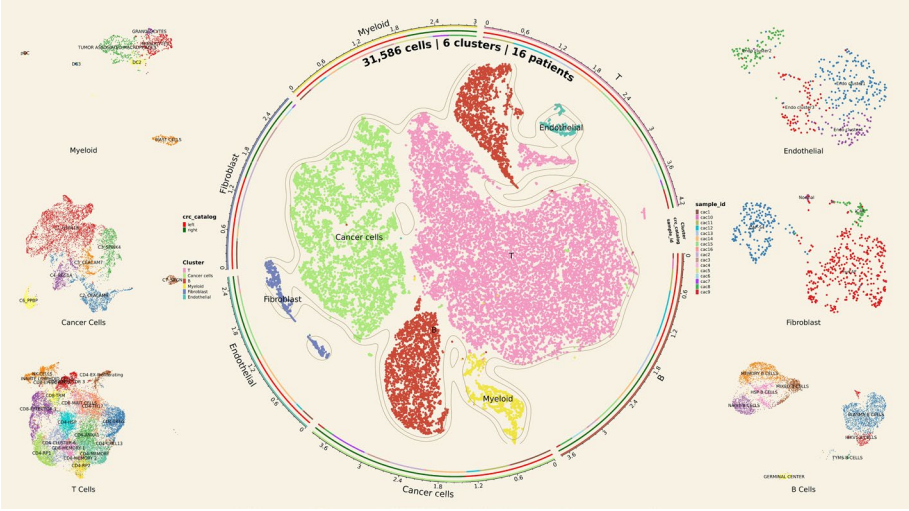

Fig. 1 Single cell atlas of RCRC and LCRC. The large central circle shows the six major cell types (epithelial cells, T cells, B cells, myeloid cells, fibroblasts, and endothelial cells). Surrounding the central plot are the embeddings of subclusters within each of the six major cell types, highlighting finer cellular heterogeneity

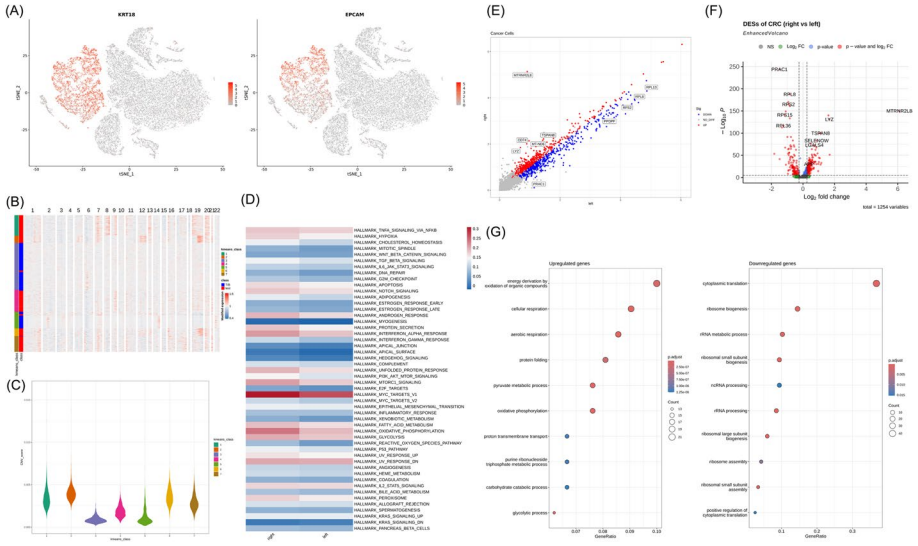

Fig. 2 Overall differences between RCRC and LCRC tumor cells. **A** Feature plot of two marker genes for epithelial cells. **B** The result of inferCNV. **C** Violin plot of CNV scores for each cell cluster. **D** GSVA results for RCRC and LCRC tumor cells. **E** Scatter plot of expression levels of overall differential genes between RCRC and LCRC tumor cells. **F** Volcano plot of overall differential genes between RCRC and LCRC tumor cells. **G** Enrichment results of differentially expressed genes between RCRC and LCRC tumor cells

population. T and B cells, which exhibit normal CNV levels, were used as reference populations, and epithelial cells were clustered together with T and B cells using k-means based on their CNV scores. Cells clustering with T/B cells (clusters 3 and 5) were classified as normal epithelial cells, while the remaining epithelial cells (clusters 1, 2, 4, 6, and 7) were considered malignant (tumor cells). After classification, 7,026 tumor cells were retained for downstream analyses. The inferCNV results revealed clear differences in CNV profiles between malignant epithelial cells and reference T/B cells (Fig. 2B, C), supporting the distinction between tumor and non-tumor cells in our dataset.

After identifying all tumor cells (7,026 cells), in order to better understand the differences in the expression patterns of key signaling pathways between LCRC and RCRC tumor cells, we conducted gene set variation analysis (GSVA) on LCRC and RCRC tumor cells. LCRC and RCRC tumor cells exhibited distinct pathway expression patterns. Signaling pathways such as "HALLMARK_MYC_TARGETS_V1" and "HALLMARK_OXIDATIVE_PHOSPHORYLATION" showed significantly higher scores in RCRC tumor cells compared to LCRC tumor cells (Fig. 2D).

We further conducted differential gene expression analysis between RCRC tumor cells (4,479 cells) and LCRC tumor cells (2,547 cells), exploring the overall gene expression differences in tumor cells between RCRC and LCRC. We identified 126 downregulated genes and 221 upregulated genes in RCRC tumor cells compared to LCRC tumor cells. Among the upregulated genes in RCRC tumor cells, the gene *MTRNR2L8* was the most significant (p_val_adj = 1.24e-150, avg_log2FC = 6.09) (Fig. 2E, F). GO enrichment analysis of these genes revealed that the upregulated genes in RCRC tumor cells were predominantly enriched in pathways related to purine ribonucleotide metabolism, ribonucleotide metabolism, and other functional pathways. Downregulated genes were primarily enriched in pathways related to cytoplasmic translation and other functional processes (Fig. 2G).

3.3 Differences in tumor cell subpopulations between LCRC and RCRC

To further refine the differences between LCRC and RCRC tumor cells, we performed a secondary dimensionality reduction and clustering on all tumor cells. The entire set of 7,026 tumor cells was grouped into 7 subclusters. We annotated these seven cell subclusters according to their specifically expressed significant genes, including C1_HSPA1B, C2_CEACAM6, C3_SPINK4, C4_REG1A, C5_CEACAM7, C6_PPBP, C7_SRGN (Fig. 3A, B).

Among the seven tumor cell subclusters, the subclusters C6_PPBP and C4_REG1A were unique to RCRC patients, while the other five subclusters were present in both LCRC and RCRC patients. The proportion of subcluster C1_HSPA1B was significantly higher in LCRC patients (60.29%) than in RCRC patients (41.85%). Additionally, the composition of tumor cell subpopulations varied considerably across patients (Fig. 3C).

Subsequently, we computed the differentially expressed genes between the seven tumor cell subclusters of RCRC and the seven tumor cell subclusters of LCRC. The results revealed that in tumor cell subclusters such as C3_SPINK4 and C1_HSPA1B, the *MTRNR2L8* gene remained the most significantly upregulated gene in RCRC compared to LCRC, consistent with our earlier findings (C3_SPINK4: avg_log2FC = 8.16, C1_HSPA1B: avg_log2FC = 6.37) (Fig. 3D).

To delineate the biological features of the seven tumor cell subclusters, we conducted enrichment analysis on the highly expressed genes within each subcluster, identifying the active biological pathways and processes specific to each tumor cell subcluster. The results indicated that the highly expressed genes in the RCRC-specific tumor cell

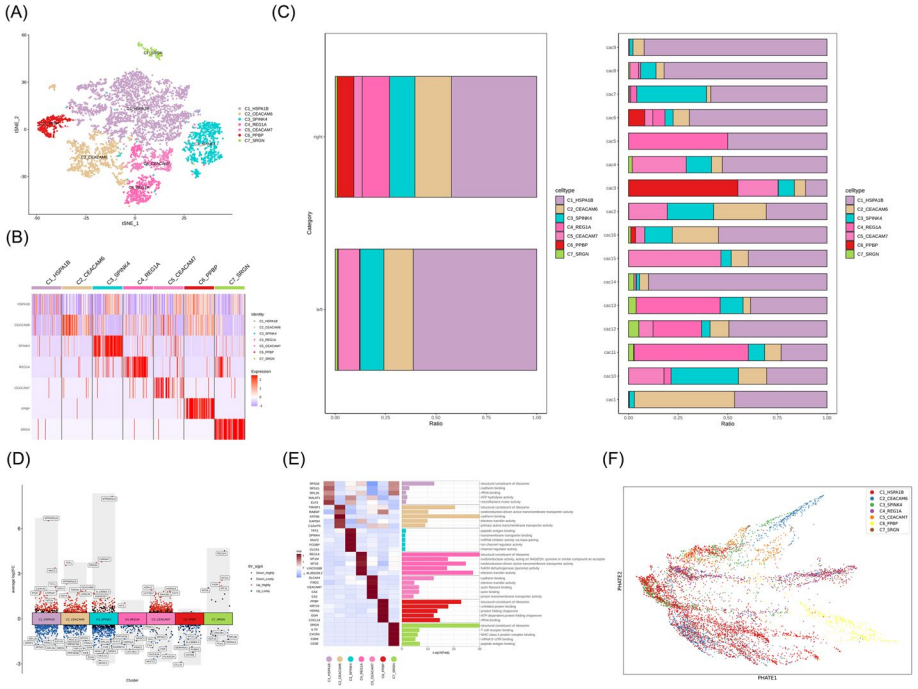

Fig. 3 Differences in tumor cell subpopulations between RCRC and LCRC. **A** t-SNE plot showing the identified subsets of all tumor cells. **B** Heatmap showing the expression of marker genes for each tumor cell subcluster. **C** Stacked bar chart showing the proportions of different tumor cell subpopulations in RCRC and LCRC, as well as in individual patient samples. **D** Scatter plot showing the differential genes in various tumor cell subpopulations between RCRC and LCRC. **E** A combined heatmap and bar chart showing the marker genes of different tumor cell subpopulations and their enriched pathways. **F** Scatter plot showing the developmental trajectories of tumor cell subpopulations inferred by PHATE

subgroups, C6_PPBP and C4_REG1A, were enriched in pathways associated with the unfolded protein response and with oxidative phosphorylation and the electron transport chain, respectively (Fig. 3E).

In addition, we constructed the developmental trajectory of tumor cells to identify the malignancy levels of different tumor cell subgroups and understand the differentiation processes between subgroups. To determine the developmental order of the seven tumor cell subgroups, we initially inferred the differentiation sequence of tumor cell subgroups using CytoTRACE. The results indicated that tumor cell subgroups such as C1_HSPA1B and C3_SPINK4 exhibited a higher degree of differentiation with lower differentiation potential, while tumor cell subgroups like C6_PPBP, C2_CEACAM6, C3_REG1A demonstrated a lower degree of differentiation with higher differentiation potential (Supplementary Fig. 3A,B).

For cells in normal tissues, cells differentiated from those with high differentiation potential and low differentiation degree to those with low differentiation potential and high differentiation degree. However, a substantial amount of research indicated that in tumor cells, cells could undergo dedifferentiation. Cells with a high degree of differentiation could transform into cells with high differentiation potential, low differentiation degree, and strong stemness. The lower the degree of differentiation, the more malignant the tumor cells became. Therefore, we defined subgroups such as C1_HSPA1B and C3_SPINK4, characterized by high differentiation and low malignancy, as the developmental starting points of tumor cells.

Based on the developmental order of tumor cell subclusters inferred by CytoTRACE, we utilized monocle2 to infer the developmental trajectory of tumor cell subclusters. The results were consistent with the predictions made by CytoTRACE, where subclusters such as C1_HSPA1B and C3_SPINK4 were positioned at the starting point of the developmental trajectory, while subclusters like C6_PPBP and C4_REG1A were located at the endpoint of the trajectory. Cells gradually developed from the State1 branch towards the State2 and State3 branches (Supplementary Fig. 3C). We conducted a developmental trajectory branch analysis to investigate the specific process of tumor cell differentiation from the initial state into two branches. A total of 779 key genes involved in the differentiation of primitive tumor cells into two directions were identified, and these genes were categorized into four clusters. Each cluster exhibited different expression patterns in the two branches. Subsequently, GO enrichment analysis was performed on the genes in each cluster. The enrichment results showed that genes upregulated in the State3 branch were enriched in pathways related to the MHC protein complex. Conversely, genes upregulated in the State2 branch were enriched in processes such as antioxidant activity, endopeptidase and peptidase inhibitor activity (Supplementary Fig. 3D).

To better illustrate the process of tumor cell development and enhance the developmental trajectory's reliability, we also employed monocle3 and PHATE to infer the tumor cells' developmental trajectory. The inference results from monocle3 and PHATE were consistent with the previous findings (Fig. 3F, Supplementary Fig. 3E).

In summary, the developmental trajectory revealed that tumor cells progressed from subpopulations with higher differentiation and lower malignancy, such as C1_HSPA1B and C3_SPINK4, towards subpopulations with lower differentiation and higher malignancy, including C6_PPBP, C4_REG1A, C2_CEACAM6, and others. Notably, the subpopulations C6_PPBP and C4_REG1A, situated at the end of the developmental

trajectory and characterized by higher malignancy, were specific to RCRC patients. In contrast, the subpopulation C1_HSPA1B, located at the starting point of the trajectory and exhibiting lower malignancy, was significantly more prevalent in LCRC than in RCRC. This further emphasized the heightened malignancy of RCRC tumor cells compared to LCRC.

3.4 Analysis of the upregulated gene *MTRNR2L8* in RCRC tumor cells

In the earlier stages of our research, we identified that the *MTRNR2L8* gene was the most significantly upregulated gene in RCRC tumor cells compared to LCRC tumor cells. Consequently, we conducted a detailed analysis of this gene to investigate whether it was a key factor contributing to the differences in survival and prognosis between LCRC and RCRC patients. Additionally, we aimed to explore the mechanisms through which this gene influenced survival and prognosis.

First, we conducted a survival analysis on the *MTRNR2L8* gene based on TCGA data using GEPIA2 to investigate whether the expression level of the *MTRNR2L8* gene impacts the survival and prognosis of CRC patients. The results revealed that elevated expression levels of the *MTRNR2L8* gene were linked to decreased survival rates among CRC patients (Log-rank test P = 0.026) (Fig. 4A). To further assess the prognostic relevance of *MTRNR2L8* while accounting for potential clinical confounders, a multivariate Cox proportional hazards regression analysis was performed in the TCGA-COAD cohort. After adjustment for age, gender, clinical stage, and treatment

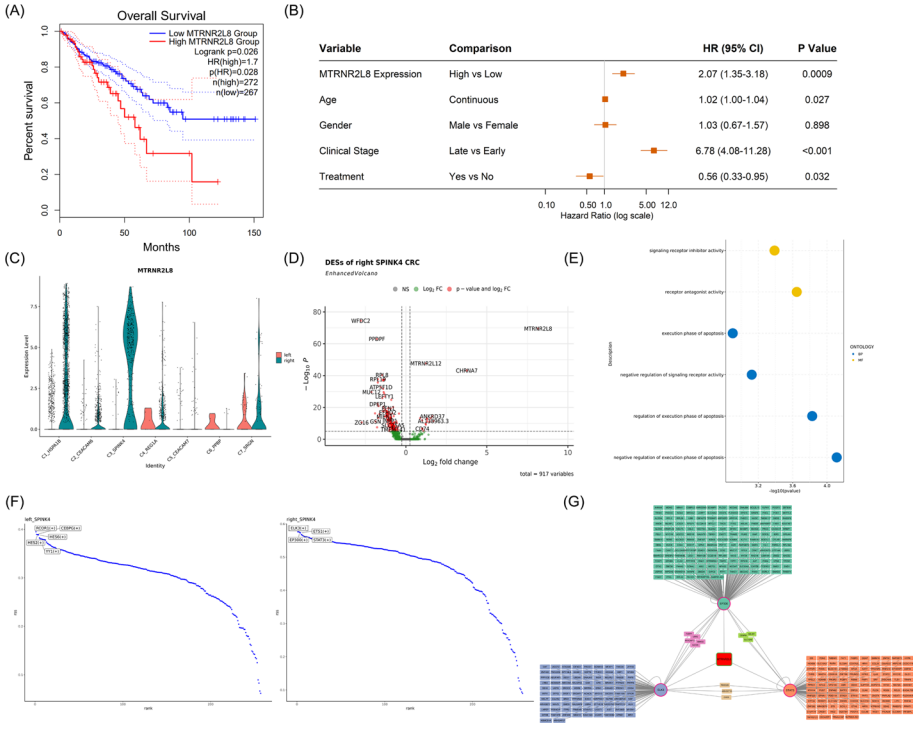

Fig. 4 Analysis of *MTRNR2L8* gene. **A** Kaplan–Meier plot showing overall survival in patients stratified based on the expression level of *MTRNR2L8* gene. **B** Violin plot showing the expression of the *MTRNR2L8* gene in RCRC tumor cell subpopulations and LCRC tumor cell subpopulations. **C** Volcano plot showing the differential genes between the C3_SPINK4 subpopulation of RCRC and the C3_SPINK4 subpopulation of LCRC. **D** Dot plot showing the enriched pathways (pathways that contain the *MTRNR2L8* gene) of upregulated genes in the C3_SPINK4 subpopulation of RCRC. **E** Top 5 transcription factors inferred by SCENIC for the C3_SPINK4 subpopulation of RCRC and LCRC. **F** Transcriptional regulatory network of the transcription factors EP300, ELK3, and STAT3, generated using Cytoscape

status, *MTRNR2L8* expression remained significantly associated with overall survival (HR = 2.07, 95% CI 1.35–3.18, P = 0.0009), indicating that *MTRNR2L8* provides prognostic information beyond standard clinicopathological variables (Fig. 4B). Therefore, the upregulation of the *MTRNR2L8* gene in RCRC tumor cells may be one of the factors contributing to the poorer prognosis of RCRC patients.

Subsequently, we examined the expression of the *MTRNR2L8* gene in the seven tumor cell subclusters of LCRC and RCRC. The findings indicated that the expression of the *MTRNR2L8* gene showed the most significant differences between LCRC and RCRC in the tumor cell subcluster C3_SPINK4 (Fig. 4C).

To further explore the specific mechanisms by which the *MTRNR2L8* gene may contribute to the poorer prognosis and survival outcomes in RCRC patients, we conducted a differential gene expression analysis between the C3_SPINK4 subcluster of RCRC and that of LCRC. The results of the differential analysis revealed that the *MTRNR2L8* gene remained the most significantly upregulated gene in the C3_SPINK4 subcluster of RCRC compared to the C3_SPINK4 subcluster of LCRC (Fig. 4D). Then, we conducted GO enrichment analysis on the upregulated genes in the C3_SPINK4 subcluster of RCRC. We extracted pathways containing the *MTRNR2L8* gene and ultimately identified that the main pathways were related to apoptosis (Fig. 4E). Hence, the *MTRNR2L8* gene may contribute to the poorer prognosis and survival of RCRC patients by influencing biological processes such as apoptosis.

To further elucidate the upstream regulatory mechanisms leading to the upregulation of the *MTRNR2L8* gene in RCRC tumor cells, we conducted a transcription factor analysis on the C3_SPINK4 subcluster of RCRC, and the C3_SPINK4 subcluster of LCRC, identifying the top five most specific transcription factors for each cell subpopulation. The five most specific transcription factors for the C3_SPINK4 subcluster of LCRC were *RCOR1*, *CEBPG*, *HES6*, *HES2*, and *YY1*. For the C3_SPINK4 subcluster of RCRC, the top five most specific transcription factors were *TCF12*, *ELK3*, *ETS1*, *EP300*, and *STAT3* (Fig. 4F).

Intriguingly, we found that among the top five most specific transcription factors for the C3_SPINK4 subcluster of RCRC, three transcription factors had a regulatory role on the *MTRNR2L8* gene. These were *STAT3*, *ELK3*, and *EP300*. Therefore, we further constructed a transcriptional regulatory network using Cytoscape, revealing that *MTRNR2L8* was the only gene co-regulated by these three transcription factors (Fig. 4G).

3.5 Validation of the *MTRNR2L8* gene

We first validated the expression difference of the *MTRNR2L8* gene between LCRC and RCRC tumor cells using bulk RNA-seq data from the TCGA colorectal cancer cohort, which included 297 LCRC samples and 218 RCRC samples. Using edgeR, we performed differential expression analysis on the bulk RNA-seq data of LCRC and RCRC, identifying a total of 4596 upregulated genes and 1,497 downregulated genes in RCRC compared to LCRC. Notably, *MTRNR2L8* was among the upregulated genes (Supplementary Fig. 4A).

Furthermore, we performed a Spearman correlation analysis between the expression levels of *MTRNR2L8* and three transcription factors *ELK3*, *EP300*, and *STAT3*. The results showed a strong correlation between *MTRNR2L8* expression and *ELK3* (R = 0.3;

$P = 5.4 \times 10^{-6}$), *EP300* (R = 0.4; $P = 5.5 \times 10^{-10}$), and *STAT3* (R = 0.29; $P = 1.2 \times 10^{-5}$) (Supplementary Fig. 4B, C, D).

These results further validate the differential expression of *MTRNR2L8* between RCRC and LCRC tumor cells. The significant upregulation of *MTRNR2L8* in RCRC tumor cells may be attributed to regulatory effects exerted by transcription factors such as *ELK3*, *EP300*, and *STAT3*.

To further validate the role of *MTRNR2L8* in CRC progression, we performed qPCR experiments on tumor samples from 136 local CRC patients (Supplementary Table 1). The results showed a gradual increase in *MTRNR2L8* expression with CRC progression (Supplementary Fig. 5A). Notably, a significant difference in *MTRNR2L8* expression was observed between Stage II and Stage IV tumors (P = 0.031) (Supplementary Fig. 5B).

Subsequently, we grouped Stage I and Stage II as early-stage CRC and Stage III and Stage IV as late-stage CRC. The analysis revealed a significant difference in *MTRNR2L8* expression between the early- and late-stage groups (P = 0.046) (Supplementary Fig. 5C). Additionally, we examined the expression differences of *MTRNR2L8* across lymph node metastasis stages (N1 + N2 vs. N0) and found that *MTRNR2L8* expression was significantly higher in the N1 + N2 group compared to the N0 group (P = 0.041) (Supplementary Fig. 5D). These findings suggest that *MTRNR2L8* plays a significant role in CRC progression and metastasis.

3.6 Differences in T cells between LCRC and RCRC

To further investigate the differences in T cell subpopulations between LCRC and RCRC, we performed re-dimensionality reduction, clustering, subgrouping, and annotation on all T cells (16,730 cells), identifying 19 T cell subpopulations (Fig. 5A, B).

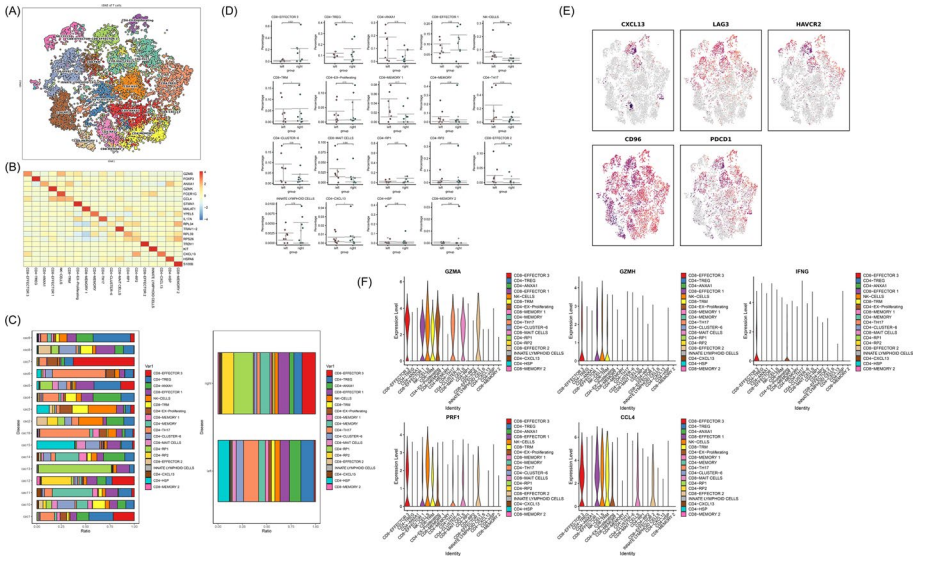

Fig. 5 Differences in T cell subpopulations between RCRC and LCRC. **A** t-SNE plot showing the identified subsets of all T cells. **B** Heatmap showing the expression of marker genes for each T cell subcluster. **C** Stacked bar chart showing the proportions of different T cell subpopulations in RCRC and LCRC, as well as in individual patient samples. **D** Differences in proportions of T cell subpopulations between RCRC (n = 8) and LCRC (n = 8) samples. Proportions were calculated per sample, and group differences were assessed using a two-sided Wilcoxon rank-sum test; p-values are shown. **E** Feature plot showing the expression of several activation or exhaustion-related genes in the CD8-EFFECTOR 3 subpopulation. **F** Violin plot showing the expression of several genes involved in mediating effector functions in the CD8-EFFECTOR 3 subpopulation

Subsequently, we calculated the proportions of the 19 T cell subpopulations. Among these 19 subpopulations, the proportions of CD4-RP1, CD4-RP2, and CD8-EFFECTOR 3 subpopulations were significantly higher in RCRC T cells compared to LCRC T cells, while the proportion of the CD4-HSP subpopulation was significantly higher in LCRC T cells compared to RCRC T cells (Fig. 5c).

To further identify the T cell subpopulations with significant proportion differences between LCRC and RCRC, we conducted significance tests on the proportion differences of the 19 T cell subpopulations between LCRC patient samples and RCRC patient samples. The results showed that the proportion differences of the CD8-EFFECTOR 3 and NK-CELLS subpopulations between LCRC patient samples and RCRC patient samples were significant. The CD8-EFFECTOR 3 subpopulation had a higher proportion in RCRC patient samples, while the NK-CELLS subpopulation had a higher proportion in LCRC patient samples (Fig. 5D).

We subsequently conducted further analysis on the CD8-EFFECTOR 3 subpopulation. The CD8-EFFECTOR 3 subpopulation expressed *GZMA*, *GZMH*, *IFNG*, *PRF1*, and *CCL4*, which have been proven to mediate effector functions [29–32] (Fig. 5F). Interestingly, the CD8-EFFECTOR 3 subpopulation also expressed marker genes associated with activation (*CXCL13*) as well as exhaustion (*LAG3*, *HAVCR2*, *CD96*, *PDCD1*) (Fig. 5E). To further characterize the biological features of the CD8-EFFECTOR 3 subpopulation, we performed GO and KEGG enrichment analyses on the genes specifically expressed in this subpopulation. The KEGG enrichment analysis results indicated that these marker genes were primarily enriched in pathways such as Antigen Processing and Presentation, Cell Adhesion Molecules, and Natural Killer Cell-Mediated Cytotoxicity. The GO enrichment analysis results revealed that these marker genes were mainly enriched in processes such as Regulation of T Cell Activation, Leukocyte Cell–Cell Adhesion, and Negative Regulation of Immune System Process (Supplementary Fig. 6). Therefore, the above results suggested that the CD8-EFFECTOR 3 subpopulation was in an immune activation state while also exhibiting signs of exhaustion.

To validate the proportional differences of the CD8-EFFECTOR 3 subpopulation between LCRC and RCRC, we analyzed the single-cell transcriptomic data from the validation cohort (GSE132465). The results of dimensionality reduction and clustering revealed that all cells were classified into five clusters (Supplementary Fig. 7A). Based on specific marker genes, we annotated the five cell populations to known cell types (Supplementary Fig. 7B).

We extracted T cells for further dimensionality reduction and clustering, resulting in 13 subpopulations of T cells (Supplementary Fig. 8A, B). Subsequently, we calculated the proportions of these subpopulations in the LCRC and RCRC patient samples. The results confirmed our previous findings, showing that the proportion of CD8 + Effector 3 subpopulation, which simultaneously expresses exhaustion and cytotoxicity genes, was significantly higher in RCRC T cells compared to LCRC T cells (Supplementary Fig. 8C, D).

To confirm the presence of cell subpopulations simultaneously expressing immune activation and exhaustion genes within the CRC microenvironment, we analyzed a spatial transcriptomic dataset of colorectal cancer. Immune exhaustion genes such as *PDCD1* and *CD96*, along with immune activation genes such as *CXCL13* and *PRF1*, showed spatial co-localization with high expression levels in specific tissue regions

(Fig. 6). This spatial co-expression pattern supports the existence of functionally complex immune subpopulations, such as the CD8-EFFECTOR 3 subset, within localized areas of the tumor microenvironment.

Additionally, to explore the overall gene expression differences between RCRC T cells and LCRC T cells, we performed differential expression analysis on RCRC T cells (6472 cells) and LCRC T cells (10258 cells). We identified 177 downregulated genes and 83 upregulated genes in RCRC T cells compared to LCRC T cells. The genes that were upregulated in RCRC T cells included *CXCL13*, *IFITM1*, *IGKC*, and others. In contrast, the genes that were upregulated in LCRC T cells primarily included heat shock genes such as *HSPA1A*, *HSPA1B*, *HSPA6*, and others (Supplementary Fig. 9A). The upregulated genes in RCRC T cells were mainly enriched in GO pathways such as humoral immune response and immunoglobulin receptor binding, as well as KEGG pathways like antigen processing and presentation (Supplementary Fig. 9B). The downregulated genes were mainly enriched in GO pathways such as protein folding and heat shock protein binding, as well as KEGG pathways including apoptosis and IL-17 signaling pathway (Supplementary Fig. 9C).

3.7 Differences in myeloid cells between LCRC and RCRC

Next, we analyzed the differences between LCRC myeloid cells (608 cells) and RCRC myeloid cells (361 cells). All myeloid cells were further subdivided into 7 myeloid cell subgroups (Supplementary Fig. 10A, B).

We calculated the proportions of the seven myeloid cell subgroups and found that the proportion of TUMOR-ASSOCIATED MACROPHAGES (TAMs) was higher in RCRC,

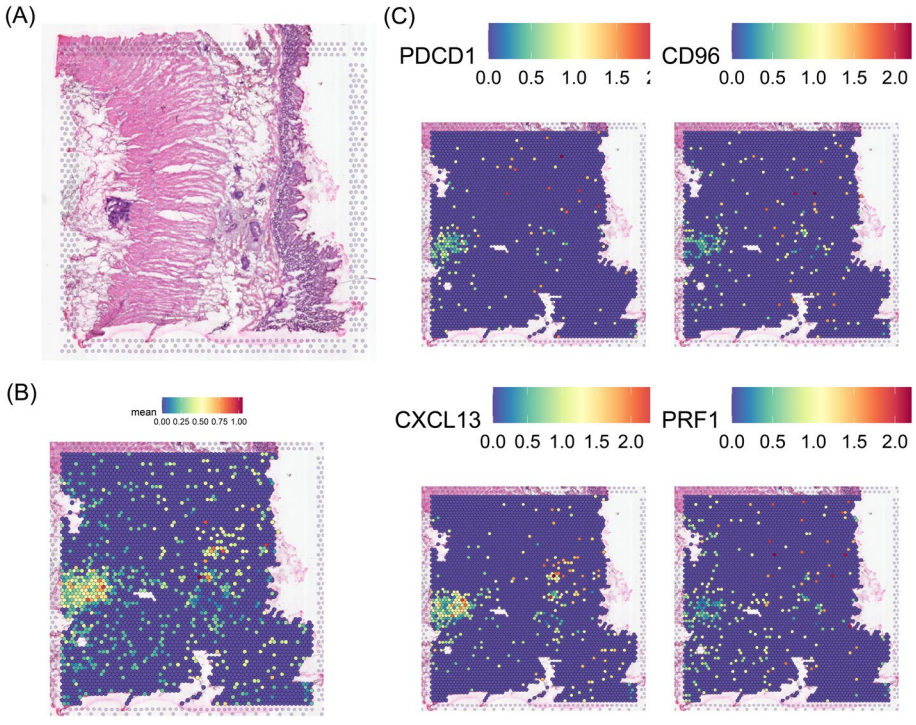

Fig. 6 Spatial transcriptomic evidence for the presence of CD8-EFFECTOR 3 T cell subpopulations in the CRC tumor microenvironment. **A** Original image of the CRC tumor tissue section. **B** Spatial plot showing the average expression of four key genes (*PDCD1*, *CD96*, *CXCL13*, and *PRF1*), indicative of co-expression of immune exhaustion and activation markers. **C** Individual spatial expression patterns of *PDCD1*, *CD96*, *CXCL13*, and *PRF1*

while the proportion of MONOCYTES was higher in LCRC (Supplementary Fig. 10C). Significance testing demonstrated that the difference in TAMs proportions between LCRC and RCRC was statistically significant (Supplementary Fig. 10D).

Notably, certain genes associated with a pro-inflammatory phenotype, such as *S100A8* and *S100A9* [33, 34], were highly expressed in the MONOCYTES subgroup (Supplementary Fig. 10E). Additionally, the TAMs subgroup highly expressed genes associated with anti-inflammatory characteristics, such as *APOE* and *CD163* [35–37] (Supplementary Fig. 10F).

We also performed differential analysis of LCRC and RCRC myeloid cells, identifying 42 downregulated genes and 18 upregulated genes in RCRC myeloid cells compared to LCRC myeloid cells. The upregulated genes mainly include *APOE*, *APOC1*, *SPP1*, and *CCL18* (Supplementary Fig. 11A). The upregulated genes in RCRC myeloid cells were primarily enriched in GO pathways such as immunoglobulin-mediated immune response and cell junction disassembly, as well as KEGG pathways including complement and coagulation cascades and efferocytosis (Supplementary Fig. 11B). The upregulated genes in LCRC myeloid cells were primarily enriched in GO pathways such as regulation of translation and translation regulator activity, as well as KEGG pathways including viral myocarditis and antigen processing and presentation (Supplementary Fig. 11D).

3.8 Differences in fibroblasts between LCRC and RCRC

We further analyzed the differences between LCRC fibroblasts (330 cells) and RCRC fibroblasts (313 cells). All fibroblasts were divided into 4 subgroups (Supplementary Fig. 12A,B). There were no significant differences in the proportions of the four fibroblast subgroups between LCRC and RCRC (Supplementary Fig. 12C).

Gene expression differential analysis identified 6 downregulated genes and 37 upregulated genes in RCRC fibroblasts compared to LCRC fibroblasts. The upregulated genes mainly include *HSPA6*, *HSPH1*, *SFRP2*, and *ICAM1* (Supplementary Fig. 12D). The upregulated genes in RCRC fibroblasts were primarily enriched in GO pathways such as response to unfolded protein and extrinsic apoptotic signaling pathway. The downregulated genes were mainly enriched in GO pathways including focal adhesion and cadherin binding (Supplementary Fig. 12E, F).

3.9 Differences in B cells between LCRC and RCRC

We also conducted an analysis to compare LCRC B cells (2123 cells) with RCRC B cells (2901 cells). All B cells were divided into 8 subgroups (Supplementary Fig. 13A, B). The MIXED B CELLS and PLASMA B CELLS subgroups had higher proportions in RCRC B cells compared to LCRC B cells, while the HSP B CELLS and NAIVE B CELLS subgroups had higher proportions in LCRC B cells compared to RCRC B cells (Supplementary Fig. 13C). Interestingly, the HSP B CELLS subgroup was almost exclusively present in LCRC.

Differential analysis identified 194 downregulated genes and 52 upregulated genes in RCRC B cells compared to LCRC B cells. The upregulated genes mainly include *IGKV1-16*, *IGLV1-47*, and *IGLV6-57*, while the downregulated genes primarily consist of heat shock protein genes such as *HSP90AA1*, *DNAJB1*, *HSPA1A*, and *HSPA1B* (Supplementary Fig. 13D). The upregulated genes in RCRC B cells were primarily enriched in GO

pathways such as immunoglobulin production and immunoglobulin-mediated immune response. The downregulated genes were mainly enriched in GO pathways including protein folding and response to heat (Supplementary Fig. 13E, F).

3.10 Differences in endothelial cells between LCRC and RCRC

Finally, we analyzed the differences between LCRC endothelial cells (196 cells) and RCRC endothelial cells (205 cells). All endothelial cells were divided into 4 subgroups. There were no significant differences in the proportions of these 4 endothelial cell subgroups between LCRC and RCRC (Supplementary Fig. 14A, B, C).

Subsequently, we identified differential genes between LCRC endothelial cells and RCRC endothelial cells, finding 4 downregulated genes and 5 upregulated genes in RCRC endothelial cells compared to LCRC endothelial cells. The upregulated genes were *DNAJB1*, *JUN*, *HSPA1B*, *BST2*, and *HSPA8*, while the downregulated genes were *RPS2*, *IFITM2*, *HTRA1*, and *IGFBP2* (Supplementary Fig. 14D).

3.11 Analysis of cell communication in LCRC and RCRC

To provide a more in-depth elucidation of the interactions among different cell types and their variances between LCRC and RCRC, we employed CellChat for cell communication analysis.

The results indicated that the number of interactions between fibroblasts and tumor cells in RCRC (with fibroblasts as signal ligands and tumor cells as signal receptors), as well as the number of interactions within fibroblasts, was significantly higher than in LCRC (Fig. 7A, B). Additionally, the communication level of the ligand-receptor pair *APP-CD74* was significantly higher in RCRC than in LCRC (Fig. 7C, D).

Previous studies have shown that *APP-CD74* interactions can inhibit the cleavage of APP into β-amyloid. In addition, APP plays a key role in promoting tumor cell

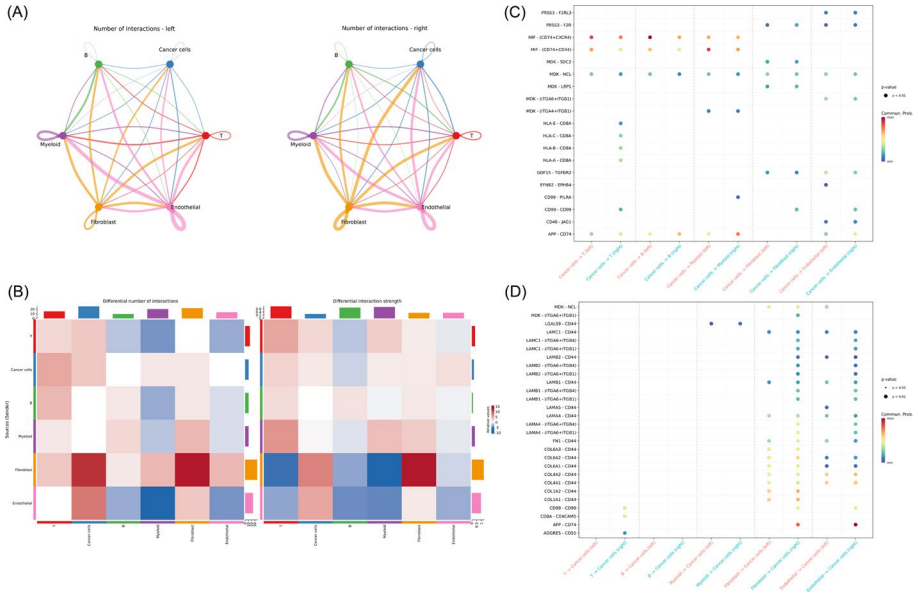

Fig. 7 Results of the cell communication analysis generated by CellChat. **A** Chord diagram showing the number of interactions among different cell types. **B** Heatmap showing the differences in the number and strength of cell–cell interactions between LCRC and RCRC. **C** Dot plot showing the interactions between tumor cells and other cell types. **D** Dot plot showing the interactions between other cell types and tumor cells

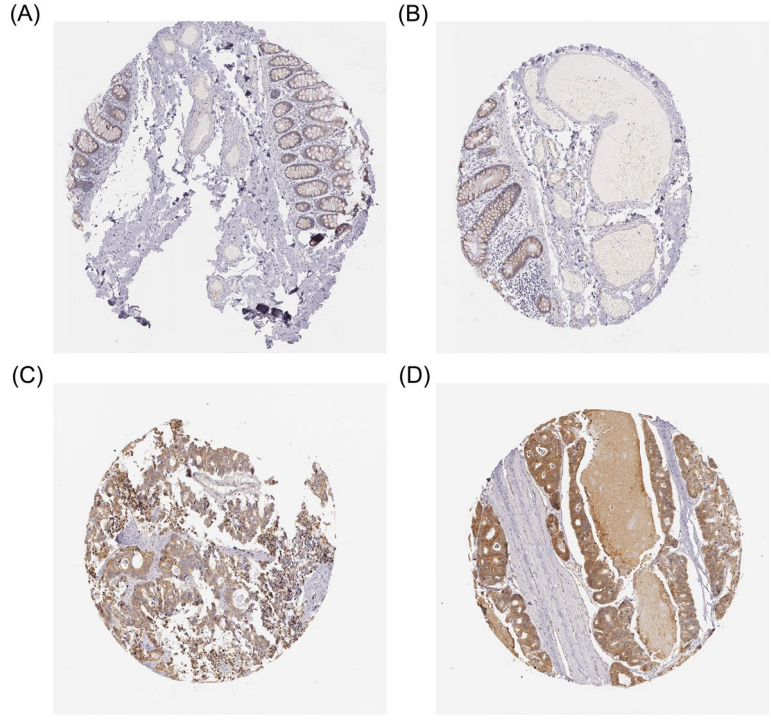

Fig. 8 Validation of APP protein accumulation in CRC tumor tissues using immunohistochemistry data from HPA. **A**, **B** IHC images of APP protein expression in normal colorectal tissues (sample IDs: 1832 and 2404). **C**, **D** IHC images of APP protein expression in colorectal tumor tissues (sample IDs: 192 and 418). All images were obtained using the HPA001462 antibody

proliferation and invasion. Therefore, the enhanced *APP-CD74* interaction observed in RCRC may lead to APP accumulation in the tumor microenvironment, potentially contributing to increased malignancy and poorer prognosis in RCRC. To validate this hypothesis, we examined immunohistochemistry data for APP protein in normal and tumor colorectal tissues from HPA database. The results showed that APP protein expression was markedly higher in tumor tissues compared to normal tissues (Fig. 8).

4 Discussion

In our study, we constructed a single-cell transcriptomic landscape highlighting the differences between LCRC and RCRC. This landscape describes the heterogeneity between LCRC and RCRC across various cell types and further identifies the associations between these molecular differences and variations in prognosis and treatment response.

Two tumor cell subclusters, C6_PPBP and C4_REG1A, were identified, both exhibited higher malignancy and were specific to RCRC. The highly expressed genes in these two subclusters were enriched in pathways related to oxidative phosphorylation and electron transport chain. Therefore, using drugs that target pathways, such as oxidative phosphorylation, may be more effective for RCRC.

Additionally, we identified *MTRNR2L8* as the most significantly upregulated gene in RCRC tumor cells compared to LCRC tumor cells. Pathway enrichment analysis further indicated that elevated *MTRNR2L8* expression was associated with transcriptional programs related to apoptotic processes in RCRC tumor cells. Transcription factor analysis revealed that *MTRNR2L8* expression was correlated with the activity of transcription factors such as *STAT3*, *ELK3*, and *EP300*, suggesting potential upstream regulatory

associations. These expression and association patterns were further supported by analyses of TCGA datasets. Additionally, qPCR experiments on locally collected CRC samples revealed that *MTRNR2L8* expression levels increased with tumor stage and were higher in metastatic tumors compared to non-metastatic ones. Together, these results indicate that *MTRNR2L8* is a risk-associated marker, with higher expression observed in RCRC, advanced tumor stages, and metastatic tumors.

Supporting evidence from previous studies further suggests potential functional roles of *MTRNR2L8* in cancer. Single-cell analysis in colorectal cancer has shown that *MTRNR2L8* is highly expressed in exhausted CD8 + T cells, particularly in right-sided tumors, and may be involved in T cell differentiation and patient prognosis through interactions with Treg, proliferative, invasive, and endothelial cells (CXCL13 and TGFB-TGFBR signaling) [38]. In hepatocellular carcinoma, *MTRNR2L8* was identified as the most important feature in a predictive exosomal RNA signature, highlighting its potential relevance in cancer risk stratification [39]. Moreover, studies on CD19 CAR-T cells revealed that *MTRNR2L8*, encoding the Humanin-like 8 peptide, can regulate metabolic fitness and anti-apoptotic programs, suggesting a role in cell survival and apoptosis regulation [40]. Collectively, these findings support the notion that *MTRNR2L8* may contribute to cellular programs associated with tumor progression and risk, consistent with our observations in this study.

Through the analysis of T cells, we found that the proportion of the CD8-EFFECTOR 3 subpopulation differed significantly between LCRC and RCRC patient samples. By conducting additional analysis of the CD8-EFFECTOR 3 subpopulation, we discovered that this subpopulation exhibited high expression of marker genes related to both activation (*CXCL13*) and exhaustion (*LAG3*, *HAVCR2*, *CD96*, *PDCD1*). *CXCL13* promotes the formation of tertiary lymphoid structures (TLS) and functional immune responses by attracting B cells and follicular helper T cells. In the tumor microenvironment, the presence of *CXCL13* and TLS is associated with stronger anti-tumor immune responses and better prognosis [41–44]. *LAG3* transmits inhibitory signals to T cells by binding to its ligand, thereby suppressing T cell function. In cancer, tumor cells can upregulate the expression of *LAG3* and its ligands to inhibit T cell anti-tumor activity, helping tumor cells evade attacks from the immune system [45–48]. *HAVCR2* also transmits inhibitory signals by binding to its ligand, leading to T cell exhaustion. By suppressing the function of anti-tumor T cells and NK cells, *HAVCR2* supports tumor cell survival and proliferation [49–51]. By binding to its ligands *PD-L1* or *PD-L2*, *PD-1* transmits inhibitory signals that reduce T cell proliferation and cytokine secretion, leading to T cell exhaustion [52–54]. The high expression of *CXCL13* indicates that the CD8-EFFECTOR 3 subpopulation is in an activated state, possibly actively participating in immune responses. At the same time, the elevated expression of negative immune regulatory molecules such as *LAG3*, *HAVCR2*, *CD96*, and *PDCD1* suggests that CD8-EFFECTOR 3 cells are also exhibiting signs of immune exhaustion, rendering them unable to sustain effective tumor cell killing. Furthermore, through the single-cell transcriptomic data from the validation cohort, we also confirmed the proportional differences of the T cell subpopulations, which simultaneously express exhaustion and cytotoxicity genes, between LCRC and RCRC.

In summary, the significantly higher proportion of the CD8-EFFECTOR 3 subpopulation in RCRC compared to LCRC may indicate that RCRC patients are more sensitive to

immune checkpoint inhibitors than LCRC patients. Specifically, since the CD8-EFFECTOR 3 subpopulation highly expresses immune checkpoint proteins such as *LAG3*, *HAVCR2*, and *PDCD1*, simultaneously targeting multiple immune checkpoints by using a combination of checkpoint inhibitors may overcome resistance to a single drug, enhancing treatment efficacy and improving response rates in RCRC patients.

Interestingly, we also identified a T cell subpopulation, CD4-HSP, that is almost exclusively present in LCRC and highly expresses certain heat shock genes. Recent studies have identified a T cell subpopulation, T_{STR}, through pan-cancer analysis, which also highly expresses heat shock genes and has been shown to be associated with adverse responses to immune checkpoint inhibitor therapy, representing a unique resistance mechanism to such treatments [55]. This is consistent with our findings, which identified a T cell subpopulation, CD4-HSP, that is unique to LCRC and is nearly absent in RCRC. This further suggests that the poor response to immune checkpoint inhibitor therapy in LCRC may be due to the presence of the CD4-HSP T cell subpopulation.

For myeloid cells, we found that the proportion of the MONOCYTES subpopulation in all LCRC myeloid cells was significantly higher than in all RCRC myeloid cells, while the proportion of the TUMOR-ASSOCIATED MACROPHAGES (TAMs) subpopulation was higher in all RCRC myeloid cells compared to all LCRC myeloid cells. We also found that the MONOCYTES subpopulation highly expresses genes associated with a pro-inflammatory phenotype, indicating a strong pro-inflammatory profile. The TAMs subpopulation exhibited high expression of genes associated with anti-inflammatory characteristics, such as *APOE* and *CD163*, suggesting that this TAM subpopulation corresponds to M2-type macrophages. M2 macrophages promote tumor immune suppression and tumor progression by enhancing tumor angiogenesis or indirectly inducing interactions among immune cells in the tumor microenvironment [56, 57]. Therefore, the significantly higher proportion of TAMs in RCRC compared to LCRC may be one of the reasons for the poorer prognosis in RCRC. This also suggests that for RCRC patients, using drugs that target TAMs may be more effective, potentially enhancing immunotherapy and improving the prognosis of RCRC patients.

Differential analysis of LCRC and RCRC myeloid cells revealed that the genes most upregulated in RCRC myeloid cells include *APOE*, *APOC1*, *SPP1*, and *CCL18*. *APOE* is a known anti-inflammatory gene [35]. It has been reported that *APOC1* is associated with cancer progression and promotes tumor cell proliferation, migration, and invasion [58]. Additionally, *APOC1* levels are correlated with M2 tumor-associated macrophages (TAMs), serving as an immune biomarker that regulates macrophage polarization and promotes tumor metastasis [59]. Studies have shown that inhibiting *APOC1* expression can promote the conversion of M2 macrophages to M1 macrophages through ferroptosis and enhance the efficacy of anti-PD-1 immunotherapy [60]. Therefore, for RCRC, combining *APOC1* inhibition with immunotherapy may yield better outcomes. Research has found that *SPP1* expression in TAMs is associated with poor tumor prognosis and chemotherapy resistance [61]. Moreover, other studies have indicated that SPP1 + macrophages may be linked to cellular senescence, contributing to poor tumor prognosis [62]. Thus, the high expression of *SPP1* in RCRC myeloid cells may be one of the reasons for the poorer prognosis and reduced response to chemotherapy in RCRC patients. Studies have shown that *CCL18* is a biomarker of poor tumor prognosis. TAM-derived *CCL18* can promote tumor cell metastasis [63, 64]. Additionally, research has confirmed

that *CCL18* can induce the maturation of monocytes into M2 macrophages [65]. Therefore, the high expression of *CCL18* in RCRC myeloid cells may be one of the reasons for the poorer prognosis and the higher proportion of TAMs in RCRC.

For fibroblasts, the differential analysis revealed that genes such as *HSPA6*, *HSPH1*, *SFRP2*, and *ICAM1* were upregulated in RCRC fibroblasts. Studies have shown that *WNT16B* is a therapy-induced modulator of chemotherapy sensitivity [66], and the expression of *SFRP2* in fibroblasts can enhance *WNT16B* signaling, increasing tumor resistance to chemotherapy [67]. Therefore, the upregulation of *SFRP2* in RCRC fibroblasts may contribute to the poor response of RCRC to chemotherapy. In addition, literature reports that *ICAM1* expression in fibroblasts can promote the progression of colorectal cancer by activating *AKT* and *STAT3* [68]. Thus, the upregulation of *ICAM1* in RCRC fibroblasts may also contribute to the higher malignancy and poorer prognosis of RCRC.

By analyzing B cells, we discovered a B cell subpopulation, HSP B CELLS, which is nearly exclusive to LCRC and absent in RCRC. However, studies on this B cell subpopulation characterized by high HSP gene expression remain scarce, and its influence on tumor prognosis and treatment response warrants further investigation. Additionally, differential analysis revealed that genes such as *IGKV1-16*, *IGLV1-47*, and *IGLV6-57* were upregulated in RCRC B cells. These genes are all immunoglobulin-related, and their high expression in RCRC B cells may reflect the active state of B cells in the tumor microenvironment, suggesting a better response to immune checkpoint inhibitor therapy in RCRC.

Cell communication analysis revealed that the communication level of the *APP-CD74* ligand-receptor pair was significantly higher in RCRC than in LCRC. The APP protein, under the action of specific enzymes, can be cleaved to produce β-amyloid, which is associated with neurodegenerative diseases such as Alzheimer's. Previous studies have reported that the interaction between *APP* and *CD74* can inhibit the production of β-amyloid [69]. Additionally, APP protein has been shown to promote the proliferation of cancer cells in colorectal cancer and breast cancer, playing an important role in tumor cell proliferation and invasion [70–72]. Therefore, our results suggest that the relatively stronger interaction between *APP* and *CD74* in RCRC may prevent the cleavage of APP protein into β-amyloid, potentially leading to the accumulation of APP protein in the RCRC tumor microenvironment. This accumulation of APP protein may further promote tumor cell proliferation and invasion, contributing to the higher malignancy and poorer prognosis of RCRC tumor cells.

However, our study has some limitations. First, the conclusions drawn from this research require further experimental validation, including functional perturbation of key genes (e.g., knockdown or overexpression of *MTRNR2L8* in CRC cell lines or organoids with apoptosis- and stress-related readouts), co-culture assays to interrogate prioritized ligand–receptor interactions (such as the *APP–CD74* axis) with immune functional endpoints, and spatially resolved validation approaches (e.g., RNAscope or multiplex immunofluorescence) to confirm the localization of key cell states. Second, the data used in this study are relatively limited in size, and it would be beneficial to further validate our findings by integrating additional single-cell transcriptomic datasets from LCRC and RCRC.

In conclusion, our findings provide important insights into the distinct molecular and cellular characteristics between LCRC and RCRC, highlighting potential therapeutic targets and strategies that may improve treatment outcomes, particularly in RCRC patients.

Abbreviations

LCRC	Left-sided colorectal cancer
RCRC	Right-sided colorectal cancer
MTRNR2L8	Homo sapiens MT-RNR2-like 8
CD	Cluster of differentiation
HSP	Heat shock proteins
APP	Amyloid precursor protein
STAT3	Signal transducer and activator of transcription 3
ELK3	ETS-domain protein
EP300	E1A binding protein p300
qPCR	Quantitative real-time polymerase chain reaction
HPA	The Human Protein Atlas
TCGA	The Cancer Genome Atlas

Supplementary Information

The online version contains supplementary material available at https://doi.org/10.1007/s12672-026-04789-5.

Supplementary material 1: Figure 1. Expression of marker genes for the six major cell populations. Figure 2. The proportions of the six main cell populations in RCRC and LCRC, as well as in individual patient samples. Figure 3. Results of the inferred developmental trajectories of tumor cell subpopulations. Figure 4. The validation results for the *MTRNR2L8* gene using TCGA data. Figure 5. The qPCR validation results of the *MTRNR2L8* gene based on tumor samples from local CRC patients. Figure 6. GO and KEGG enrichment results for genes specifically expressed in the CD8-EFFECTOR 3 subpopulation. Figure 7. The preliminary dimensionality reduction and clustering results of the single-cell transcriptomic data from the validation cohort. Figure 8. The validation results of the proportional differences of the CD8-EFFECTOR 3 subpopulation between LCRC and RCRC. Figure 9. Overall differential genes between T cells in RCRC and LCRC, along with the enrichment results for these genes. Figure 10. Differences in Myeloid subpopulations between LCRC and RCRC. Figure 11. Overall differential genes between Myeloid in RCRC and LCRC, along with the enrichment results for these genes. Figure 12. Differences in fibroblasts between RCRC and LCRC. Figure 13. Differences in B cells between RCRC and LCRC. Figure 14. Differences in endothelial cells between RCRC and LCRC.

Supplementary material 2: Table 1. The qPCR experimental results of the *MTRNR2L8* gene in local samples. Table 2. Patient information of dataset used in this paper. Table 3. DNA primer sequence for qPCR.

Acknowledgements

We would like to thank all the patients who contributed to this study by providing their tissue samples. We also gratefully acknowledge the support from the School of Public Health and Emergency Management at Southern University of Science and Technology. Special thanks to the research teams for their assistance in data collection and analysis. We also appreciate the insightful comments and suggestions from our colleagues and reviewers.

Author contributions

Conceptualization, Chengzhi Zhao; Data curation, Yang Li and Jiachun Lv; Formal analysis, Chengzhi Zhao; Investigation, Weiye Zhou; Methodology, Chengzhi Zhao, Chuan Shi and Haibei Ma; Project administration, Xiaohua Liang and Shenying Fang; Supervision, Xiaohua Liang and Shenying Fang; Validation, Guangjian Zeng and Yeen Huang; Visualization, Chuan Shi and Haibei Ma; Writing—original draft, Chengzhi Zhao and Weiye Zhou.

Funding

This research was funded by the leading Talents Program of Guangdong Province (Grant No. 2023CX10Y002) and the National Health Commission Key Laboratory of Nuclear Technology Medical Transformation (Grant No. 2025HYX026).

Data availability

The single-cell transcriptomic data used in this study were obtained from the National Center for Biotechnology Information's Gene Expression Omnibus under the accession numbers GSE200997 (discovery cohort) and GSE132465 (validation cohort). The bulk RNA-seq data used in this study were obtained from TCGA-COAD and TCGA-READ cohorts. Spatial transcriptomic data used for validation were obtained from http://www.cancerdiversity.asia/scCRLM/. Immunohistochemistry data were retrieved from the HPA database.

Declarations

Ethics approval and consent to participate

All experimental protocols involving human tissue samples were approved by the Ethics Committee of the School of Medicine, Southern University of Science and Technology. All methods were carried out in accordance with relevant guidelines and regulations. Informed consent was obtained from all participants and/or their legal guardians.

Consent for publication

Not applicable.

Competing interests
The authors declare no competing interests.

Author details
[1]School of Public Health and Emergency Management, Southern University of Science and Technology, No. 1088, Xueyuan Blvd., Nanshan District, Shenzhen, Guangdong, People's Republic of China
[2]Department of Systems Biology for Medicine, School of Basic Medical Sciences, Fudan University, Shanghai, China
[3]Department of Gastrointestinal Surgery, Second Clinical Medical College of Jinan University, Shenzhen People's Hospital, Shenzhen, China
[4]Collaborative Innovation Center for Environmental Toxicity, School of Public Health, The Institute for Chemical Carcinogenesis, Guangzhou Medical University, Guangzhou, China
[5]Department of Epidemiology and BiostatisticsNational Clinical Research Center for Child Health and DisordersChongqing Key Laboratory of Pediatrics, Children's Hospital of Chongqing Medical University, Ministry of Education Key Laboratory of Child Development and Disorders, No.136 2nd Zhongshan Road, Yuzhong District, Chongqing 400014, China

Received: 17 November 2025 / Accepted: 3 March 2026
Published online: 17 March 2026

References

1. Bray F, Ferlay J, Soerjomataram I, Siegel RL, Torre LA, Jemal A. Global cancer statistics 2018: GLOBOCAN estimates of incidence and mortality worldwide for 36 cancers in 185 countries. CA Cancer J Clin. 2018;68(6):394–424.
2. Boisen M, Johansen J, Dehlendorff C, Larsen J, Østerlind K, Hansen J, et al. Primary tumor location and bevacizumab effectiveness in patients with metastatic colorectal cancer. Ann Oncol. 2013;24(10):2554–9.
3. Loupakis F, Yang D, Yau L, Feng S, Cremolini C, Zhang W, et al. Primary tumor location as a prognostic factor in metastatic colorectal cancer. J Natl Cancer Inst. 2015;107(3):dju427.
4. Petrelli F, Tomasello G, Borgonovo K, Ghidini M, Turati L, Dallera P, et al. Prognostic survival associated with left-sided vs right-sided colon cancer: a systematic review and meta-analysis. JAMA Oncol. 2017;3(2):211–9.
5. Benedix F, Kube R, Meyer F, Schmidt U, Gastinger I, Lippert H. Comparison of 17,641 patients with right-and left-sided colon cancer: differences in epidemiology, perioperative course, histology, and survival. Dis Colon Rectum. 2010;53(1):57–64.
6. Meguid RA, Slidell MB, Wolfgang CL, Chang DC, Ahuja N. Is there a difference in survival between right-versus left-sided colon cancers? Ann Surg Oncol. 2008;15:2388–94.
7. Carethers JM. One colon lumen but two organs. Gastroenterology. 2011;141(2):411.
8. Fearon ER. Molecular genetics of colorectal cancer. Annu Rev Pathol Mech Dis. 2011;6(1):479–507.
9. Glebov OK, Rodriguez LM, Nakahara K, Jenkins J, Cliatt J, Humbyrd C-J, et al. Distinguishing right from left colon by the pattern of gene expression. Cancer Epidemiol Biomark Prev. 2003;12(8):755–62.
10. Network CGA. Comprehensive molecular characterization of human colon and rectal cancer. Nature. 2012;487(7407):330.
11. Baran B, Ozupek NM, Tetik NY, Acar E, Bekcioglu O, Baskin Y. Difference between left-sided and right-sided colorectal cancer: a focused review of literature. Gastroenterol Res. 2018;11(4):264.
12. Khaliq AM, Erdogan C, Kurt Z, Turgut SS, Grunvald MW, Rand T, et al. Refining colorectal cancer classification and clinical stratification through a single-cell atlas. Genome Biol. 2022;23(1):113.
13. Lee H-O, Hong Y, Etlioglu HE, Cho YB, Pomella V, Van den Bosch B, et al. Lineage-dependent gene expression programs influence the immune landscape of colorectal cancer. Nat Genet. 2020;52(6):594–603.
14. Hao Y, Hao S, Andersen-Nissen E, Mauck WM, Zheng S, Butler A, et al. Integrated analysis of multimodal single-cell data. Cell. 2021;184(13):3573–87.
15. Wolf FA, Angerer P, Theis FJ. SCANPY: large-scale single-cell gene expression data analysis. Genome Biol. 2018;19:1–5.
16. Wu T, Hu E, Xu S, Chen M, Guo P, Dai Z, et al. clusterProfiler 4.0: a universal enrichment tool for interpreting omics data. Innovation N Y. 2021. https://doi.org/10.1016/j.xinn.2021.100141.
17. Hänzelmann S, Castelo R, Guinney J. GSVA: gene set variation analysis for microarray and RNA-seq data. BMC Bioinform. 2013;14:1–15.
18. Qiu X, Hill A, Packer J, Lin D, Ma Y-A, Trapnell C. Single-cell mRNA quantification and differential analysis with Census. Nat Methods. 2017;14(3):309–15.
19. Cao J, Spielmann M, Qiu X, Huang X, Ibrahim DM, Hill AJ, et al. The single-cell transcriptional landscape of mammalian organogenesis. Nature. 2019;566(7745):496–502.
20. Gulati GS, Sikandar SS, Wesche DJ, Manjunath A, Bharadwaj A, Berger MJ, et al. Single-cell transcriptional diversity is a hallmark of developmental potential. Science. 2020;367(6476):405–11.
21. Moon KR, Van Dijk D, Wang Z, Gigante S, Burkhardt DB, Chen WS, et al. Visualizing structure and transitions in high-dimensional biological data. Nat Biotechnol. 2019;37(12):1482–92.
22. Tang Z, Kang B, Li C, Chen T, Zhang Z. GEPIA2: an enhanced web server for large-scale expression profiling and interactive analysis. Nucleic Acids Res. 2019;47(W1):W556–60.
23. Van de Sande B, Flerin C, Davie K, De Waegeneer M, Hulselmans G, Aibar S, et al. A scalable SCENIC workflow for single-cell gene regulatory network analysis. Nat Protoc. 2020;15(7):2247–76.
24. Shannon P, Markiel A, Ozier O, Baliga NS, Wang JT, Ramage D, et al. Cytoscape: a software environment for integrated models of biomolecular interaction networks. Genome Res. 2003;13(11):2498–504.
25. Jin S, Guerrero-Juarez CF, Zhang L, Chang I, Ramos R, Kuan C-H, et al. Inference and analysis of cell-cell communication using CellChat. Nat Commun. 2021;12(1):1088.
26. Robinson MD, McCarthy DJ, Smyth GK. edgeR: a Bioconductor package for differential expression analysis of digital gene expression data. Bioinformatics. 2010;26(1):139–40.

27. Wu Y, Yang S, Ma J, Chen Z, Song G, Rao D, et al. Spatiotemporal immune landscape of colorectal cancer liver metastasis at single-cell level. Cancer Discov. 2022;12(1):134–53.
28. Thul PJ, Lindskog C. The Human Protein Atlas: a spatial map of the human proteome. Protein Sci. 2018;27(1):233–44.
29. Hornburg M, Desbois M, Lu S, Guan Y, Lo AA, Kaufman S, et al. Single-cell dissection of cellular components and interactions shaping the tumor immune phenotypes in ovarian cancer. Cancer Cell. 2021;39(7):928-44. e6.
30. Oh DY, Kwek SS, Raju SS, Li T, McCarthy E, Chow E, et al. Intratumoral CD4+ T cells mediate anti-tumor cytotoxicity in human bladder cancer. Cell. 2020;181(7):1612–25.
31. Wei Y, Lin C, Li H, Xu Z, Wang J, Li R, et al. CXCL13 expression is prognostic and predictive for postoperative adjuvant chemotherapy benefit in patients with gastric cancer. Cancer Immunol Immunother. 2018;67:261–9.
32. Zhang L, Yu X, Zheng L, Zhang Y, Li Y, Fang Q, et al. Lineage tracking reveals dynamic relationships of T cells in colorectal cancer. Nature. 2018;564(7735):268–72.
33. Ryckman C, Vandal K, Rouleau P, Talbot M, Tessier PA. Proinflammatory activities of S100: proteins S100A8, S100A9, and S100A8/A9 induce neutrophil chemotaxis and adhesion. J Immunol. 2003;170(6):3233–42.
34. Wang S, Song R, Wang Z, Jing Z, Wang S, Ma J. S100A8/A9 in inflammation. Front Immunol. 2018;9:1298.
35. Bach-Ngohou K, Nazih H, Nazih-Sanderson F, Zair Y, Le Carrer D, Krempf M, et al. Negative and independent influence of apolipoprotein E on C-reactive protein (CRP) concentration in obese adults. Potential anti-inflammatory role of apoE in vivo. Int J Obes. 2001;25(12):1752–8.
36. Kowal K, Silver R, Sławińska E, Bielecki M, Chyczewski L, Kowal-Bielecka O. CD163 and its role in inflammation. Folia Histochem Cytobiol. 2011;49(3):365–74.
37. Moestrup S, Møller H. CD163: a regulated hemoglobin scavenger receptor with a role in the anti-inflammatory response. Ann Med. 2004;36(5):347–54.
38. Lu J, Li Y, Yang J, Ke Z, Xu Q. Single-cell analysis reveals immune profile of T cell exhaustion-associated microenvironment in colorectal cancer. Medp Oncol. 2024;3(2):mpo-202409001.
39. Yap JYY, Goh LSH, Lim AJW, Chong SS, Lim LJ, Lee CG. Machine learning identifies a signature of nine exosomal RNAs that predicts hepatocellular carcinoma. Cancers. 2023;15(14):3749.
40. Naderinezhad S, Noble J, Savid-Frontera C, Fang B, Menges M, Koomen J, et al. Humanin-like 8 regulates metabolic fitness and anti-apoptotic programming in CD19 CAR-T cells. Blood. 2025;146:5906.
41. Hussain M, Adah D, Tariq M, Lu Y, Zhang J, Liu J. CXCL13/CXCR5 signaling axis in cancer. Life Sci. 2019;227:175–86.
42. Kazanietz MG, Durando M, Cooke M. CXCL13 and its receptor CXCR5 in cancer: inflammation, immune response, and beyond. Front Endocrinol. 2019;10:471.
43. Pitzalis C, Jones GW, Bombardieri M, Jones SA. Ectopic lymphoid-like structures in infection, cancer and autoimmunity. Nat Rev Immunol. 2014;14(7):447–62.
44. Tokunaga R, Naseem M, Lo JH, Battaglin F, Soni S, Puccini A, et al. B cell and B cell-related pathways for novel cancer treatments. Cancer Treat Rev. 2019;73:10–9.
45. Andrews LP, Cillo AR, Karapetyan L, Kirkwood JM, Workman CJ, Vignali DA. Molecular pathways and mechanisms of LAG3 in cancer therapy. Clin Cancer Res. 2022;28(23):5030–9.
46. Nguyen LT, Ohashi PS. Clinical blockade of PD1 and LAG3—potential mechanisms of action. Nat Rev Immunol. 2015;15(1):45–56.
47. Puhr HC, Ilhan-Mutlu A. New emerging targets in cancer immunotherapy: the role of LAG3. ESMO Open. 2019;4(2):e000482.
48. Ruffo E, Wu RC, Bruno TC, Workman CJ, Vignali DAA. Lymphocyte-activation gene 3 (LAG3): the next immune checkpoint receptor. Semin Immunol. 2019;42:101305.
49. Acharya N, Sabatos-Peyton C, Anderson AC. Tim-3 finds its place in the cancer immunotherapy landscape. J Immunother Cancer. 2020. https://doi.org/10.1136/jitc-2020-000911.
50. Dixon KO, Tabaka M, Schramm MA, Xiao S, Tang R, Dionne D, et al. TIM-3 restrains anti-tumour immunity by regulating inflammasome activation. Nature. 2021;595(7865):101–6.
51. Zhao L, Cheng S, Fan L, Zhang B, Xu S. TIM-3: an update on immunotherapy. Int Immunopharmacol. 2021;99:107933.
52. Ghosh C, Luong G, Sun Y. A snapshot of the PD-1/PD-L1 pathway. J Cancer. 2021;12(9):2735.
53. Han Y, Liu D, Li L. PD-1/PD-L1 pathway: current researches in cancer. Am J Cancer Res. 2020;10(3):727.
54. Kumagai S, Togashi Y, Kamada T, Sugiyama E, Nishinakamura H, Takeuchi Y, et al. The PD-1 expression balance between effector and regulatory T cells predicts the clinical efficacy of PD-1 blockade therapies. Nat Immunol. 2020;21(11):1346–58.
55. Chu Y, Dai E, Li Y, Han G, Pei G, Ingram DR, et al. Pan-cancer T cell atlas links a cellular stress response state to immunotherapy resistance. Nat Med. 2023;29(6):1550–62.
56. Fridman WH, Pagès F, Sautès-Fridman C, Galon J. The immune contexture in human tumours: impact on clinical outcome. Nat Rev Cancer. 2012;12(4):298–306.
57. Ngambenjawong C, Gustafson HH, Pun SH. Progress in tumor-associated macrophage (TAM)-targeted therapeutics. Adv Drug Deliv Rev. 2017;114:206–21.
58. Yang S, Du J, Wang W, Zhou D, Xi X. APOC1 is a prognostic biomarker associated with M2 macrophages in ovarian cancer. BMC Cancer. 2024;24(1):364.
59. Ren L, Yi J, Yang Y, Li W, Zheng X, Liu J, et al. Systematic pan-cancer analysis identifies APOC1 as an immunological biomarker which regulates macrophage polarization and promotes tumor metastasis. Pharmacol Res. 2022;183:106376.
60. Hao X, Zheng Z, Liu H, Zhang Y, Kang J, Kong X, et al. Inhibition of APOC1 promotes the transformation of M2 into M1 macrophages via the ferroptosis pathway and enhances anti-PD1 immunotherapy in hepatocellular carcinoma based on single-cell RNA sequencing. Redox Biol. 2022;56:102463.
61. Matsubara E, Yano H, Pan C, Komohara Y, Fujiwara Y, Zhao S, et al. The significance of SPP1 in lung cancers and its impact as a marker for protumor tumor-associated macrophages. Cancers Basel. 2023;15(8):2250.
62. Yu S, Chen M, Xu L, Mao E, Sun S. A senescence-based prognostic gene signature for colorectal cancer and identification of the role of SPP1-positive macrophages in tumor senescence. Front Immunol. 2023;14:1175490.
63. She L, Qin Y, Wang J, Liu C, Zhu G, Li G, et al. Tumor-associated macrophages derived CCL18 promotes metastasis in squamous cell carcinoma of the head and neck. Cancer Cell Int. 2018;18:1–14.
64. Gao W, Li Y, Zhang T, Lu J, Pan J, Qi Q, et al. Systematic analysis of chemokines reveals CCL18 is a prognostic biomarker in glioblastoma. J Inflamm Res. 2022. https://doi.org/10.2147/jir.s357787.

65. Schraufstatter IU, Zhao M, Khaldoyanidi SK, DiScipio RG. The chemokine CCL18 causes maturation of cultured monocytes to macrophages in the M2 spectrum. Immunology. 2012;135(4):287–98.
66. Sun Y, Campisi J, Higano C, Beer TM, Porter P, Coleman I, et al. Treatment-induced damage to the tumor microenvironment promotes prostate cancer therapy resistance through WNT16B. Nat Med. 2012;18(9):1359–68.
67. Sun Y, Zhu D, Chen F, Qian M, Wei H, Chen W, et al. SFRP2 augments WNT16B signaling to promote therapeutic resistance in the damaged tumor microenvironment. Oncogene. 2016;35(33):4321–34.
68. Xue C, Gao Y, Sun Z, Li X, Zhang M, Yang Y, et al. Mesenchymal stem cells derived from adipose tissue accelerate the progression of colon cancer by inducing a MTCAF phenotype via ICAM1/STAT3/AKT axis. Front Oncol. 2022;12:837781.
69. Matsuda S, Matsuda Y, D'Adamio L. CD74 interacts with APP and suppresses the production of Aβ. Mol Neurodegener. 2009;4:1–10.
70. Lim S, Yoo BK, Kim H-S, Gilmore HL, Lee Y, Lee H-p, et al. Amyloid-β precursor protein promotes cell proliferation and motility of advanced breast cancer. BMC Cancer. 2014;14:1–12.
71. Meng JY, Kataoka H, Itoh H, Koono M. Amyloid β protein precursor is involved in the growth of human colon carcinoma cell in vitro and in vivo. Int J Cancer. 2001;92(1):31–9.
72. Tsang JY, Lee MA, Ni YB, Chan SK, Cheung SY, Chan WW, et al. Amyloid precursor protein is associated with aggressive behavior in nonluminal breast cancers. Oncologist. 2018;23(11):1273–81.

Publisher's Note